Crystalline and porous CoSe dendrimeric architectures for efficient Oxygen Evolution Reaction

Muhammad Bilal [a] , Rashid [a], Amna Altaf [a], Nadeem Baig [b], Ghayoor Abbas Chotana [c], Raja Shahid Ashraf [d], Shahid Rasool [e], Ayman Nafadi [f], Manzar Sohail [a*]

[a] *Department of Chemistry, School of Natural Sciences, National University of Sciences and Technology, H-12, Islamabad 44000, Pakistan. Email: manzar.sohail@sns.nust.edu.pk*

[b] *Interdisciplinary Research Center for Membranes and Water Security, King Fahd University of Petroleum and Minerals, Dhahran, 31261 Saudi Arabia.*

[c] *Department of Chemistry and Chemical Engineering, Syed Babar Ali School of Science and Engineering, Lahore University of Management Sciences, Lahore 54792, Pakistan.*

[d] *Department of Chemistry, Government College University Lahore 54000, Pakistan.*

[e] *School of Engineering, Newcastle University, Newcastle Upon Tyne NE1 7RU, U.K and Faculty of Engineering and Environment, Northumbria University, Newcastle Upon Tyne NE1 8ST, U.K.*

[f] *Department of Chemistry, College of Science, King Saud University, Riyadh, 11451, Saudi Arabia*

**** Corressponding Author**. Department of Chemistry, School of Natural Sciences, National University of Sciences and Technology, H-12, Islamabad 44000, Pakistan. Email: manzar.sohail@sns.nust.edu.pk*

Abstract

Development of efficient and economical electrocatalyst for oxygen evolution reaction is the key challenge to renewable energy technologies. Metal selenides are attractive candidates for electrocatalytic water oxidation because of suitable surface-active sites they provide for the reaction. Herein, we report the preparation of less explored hexagonal cobalt selenide (CoSe) for oxygen evolution reaction through facile and environmentally benign one-step hydrothermal method. Reaction conditions were precisely tailored for the development of highly crystalline and porous dendrimeric architectures of CoSe. Owing to its exclusive porous and the dendrimeric crystalline network and large electrochemical surface area, the superior CoSe electrocatalyst (that is 16H) showed excellent electrochemical activity with remarkably low overpotential (250 mV at 10 mA cm^{-2}) and very high current density (570 mA cm^{-2}) in a small potential window. The Tafel slope of 16H sample was 56 mV dec^{-1} which indicates the faster kinetics at the catalyst surfaces. Moreover, it also showed excellent stability under harsh oxidative condition in a 24-hour long stability test experiment.

Keywords

CoSe; electrocatalyst; oxygen evolution reaction; water splitting; renewable energy

1. Introduction

Electrochemical water splitting is one of the most promising approaches of converting electrical energy into chemical energy in hydrogen fuel[1-3]. Water splitting reaction includes two half reactions: hydrogen evolution reaction (HER) and oxygen evolution reaction (OER). However, a major challenging reaction in water splitting is the oxygen evolution reaction (OER). OER is kinetically sluggish due to multiple-electron transfer in complicated O-H bond breakings and subsequent O=O bond formations, which require a high overpotential[4-8]. An efficient electrocatalyst is required for reducing energy barrier and enhancing energy conversion efficiency [9]. Pioneering studies for the OER have revealed that RuO_2 and IrO_2 are promising electrocatalysts. However, their high cost and scarcity severely impede their widespread applications[10-13]. This limitation encouraged researchers to explore efficient and economic electrocatalysts for the water oxidation reaction. The reported electrocatalysts for OER include transition metal oxides, hydroxides, selenides, phosphides, nitrides, and perovskites[14-19]. Among all these transition metal chalogenideis have gained attention owing to their extraordinary chemical and physical properties, quantum size, luminescence and optical properties [20]. From the various transition metal selenides and their composites for the OER, cobalt selenides have received significant attention due to their low cost, earth abundance, chemical stabilities, and comparable efficiencies to that of IrO_2 and RuO_2[21-37]. Till now, cobalt-based catalyst, particularly cobalt selenides and oxides have gained attention owing to their higher catalytic activity and corrosion stability. To enhance the efficiency of Cobalt-based

electrocatalyst, synthetic strategies has been varied, doping and composites have also been synthesized. Although, pure cobalt selenide is found a benign catalyst for oxygen evolution reaction [38].The efficient electrocatalytic activity of cobalt selenides is due to suitable surface-active sites for water splitting. Stoichiometric $CoSe_2$ is the most reported layered cobalt selenide for oxygen evolution reaction[21, 39-42]. However, there only a few reports in literature for OER with other pure phases of cobalt selenides. These include $Co_{0.85}Se$, Co_3Se_4, Co_7Se_8, Co_9Se_8 and CoSe[40, 43-49]. The OER electrocatalytic activities of all these pure cobalt selenide phases including the current work are given in supplimentry table 1. Highly crystalline and porous architectures of suitable materials are important to expose maximum surface active sites for reactants and to enhance the electron transfer process during a reaction. Selenium is sensitive to the applied reaction conditions because it exists in multiple oxidation states. Physical properties of transition metal dichalcogenides are strongly influenced by metal cations d-elctronic configuration. In CoSe exhibits +2 charge (d_7) and it is paramagnetic in nature and this metallic nature enhance the performance of CoSe [50].

Therefore, in the current study, less explored stochiometric CoSe architectures are prepared under varying reaction conditions through environmentally benign facile one-pot hydrothermal method. The reaction conditions are optimized to produce highly crystalline, and porous CoSe architectures. Also, their detailed electrochemistry for water oxidation is investigated.

2. Experimental

Cobalt chloride hexa-hydrate, Selenium powder, hydrazine hydrate, were purchased from Sigma Aldrich and were used without further purification. Deionized water obtainbed from Milli-Q (EQ-7000) direct water purification system (Merck KGaA, Darmstadt 64297, Germany), was used for making all the solutions.

2.1 Synthesis of Cobalt Selenide Nanoparticles

A series of cobalt selenide nanoparticles were synthesized at different reaction temperatures by using one pot hydrothermal method. In a typical preparation, cobalt chloride hexa-hydrate (713.8 mg, 3 mmol) was dissolved in 20 mL of deionized water under continuous stirring. Selenium powder (236.0 mg, 3 mmol) was then slowly added into the above solution and stirred for 1 hour at room temperature. Then hydrazine hydrate (8 mL) was added dropwise at 80 °C and the resulting suspension was kept on stirring at room temperature for one hour. The solution was then transferred into autoclave (100 mL Teflon container inserted in steel jacket) followed by placing it into an oven at 180 °C for 16 hours. After cooling down the autoclave to room temperature, the resulting product was thoroughly washed with deionized water and ethanol followed by centrifugation and vacuum drying at 90 °C. A similar synthetic strategy was adopted to prepare cobalt selenide nanoparticles at different reaction times i.e. 4H, 8H, 12H and 20H. Schematic illustration of this procedure is shown in Figure S1.

2.2 Electrode Fabrication

The electrode fabrication was done by drop-casting method on fluorine tin oxide (FTO) coated glass. FTO coated glass was initially cleaned by sonicating in ethanol, then in ultrapure water and finally in acetone for 15 minutes, followed by drying at 80 °C for 30 minutes. The ink was prepared by ultra-sonicating 1 mg of electrocatalyst, 2 mL of ethanol, and two drops of binder Nafion at 60°C. FTO coated glass was heated to 100 °C for 10 minutes and drop casting of ink was made on pre-heated FTO glass using a micropipette to get uniformly coated working electrode. The functional area was kept 1 cm^2 in each fabrication of the working electrode. Finally, the coated electrodes were vacuum dried at 50 °C.

3. Characterizations

Powder X-ray diffraction (p-XRD) patterns of all prepared samples were recorded using Bourevestnik Dron-8 diffractometer (St. Petersburg 190900 , Russia) equipped with Cu-Kα radiation (λ = 1.5406 Å) operated at 20 kV and 40 mA. For morphological and elemental composition studies, scanning electron microscopy (SEM) imaging, Energy-dispersive X-ray spectroscopy (EDX) and elemental mapping were performed with a Nova Nano-SEM 450 electrom microscope (Lincoln, NE 68588, United States). Electrochemical studies were conducted on Gammry Interface 1000 electrochemical work station (Warminster, PA 18974, United Staes) using conventional three-electrode system. Various electrochemical studies, including cyclic voltammetry (CV), linear sweep voltammetry (LSV), electrochemical impedance spectroscopy (EIS), and Chronopotentiometry (CP) were conducted for each prepared material. These experiments were performed in a specialized electrochemical cell of capacity 30 mL, and the electrolyte was 1 M KOH.

4. Results and discussions

p-XRD analysis was conducted and the corresponding XRD patterns are shown in Figure 1. The XRD patterns of 4H, 8H, 12H and 16H samples shows diffraction peaks at (100), (101), (102), (110), (201), (204) [44]and these peaks were found to match with standard pattern of CoSe (JCPDS-89-2004), whereas the XRD pattern of 20H sample was found matching with the standard pattern of $Co_{0.85}Se$ (JCPDS-52-1008). From 16H to 20H slight peak shift has been observed, it is assigned to $Co_{0.85}Se$ hexagonal phase [51].All peaks were assigned to corresponding crystal planes of both phases, and no extra peaks were detected, which shows the high purity of products. But the relative intensities of peaks have been increased by increasing reaction time, due to difference in direction and alignment of planes in sample. It has been observed that by decreasing reaction time from 20H to 4H size of nanoparticles has

been decreased due to which peak broadening has been occurred [52]. The reaction time longer than 16H generated vacancies in cobalt selenide, resulting in the formation of nonstoichiometric cobalt selenide, $Co_{0.85}Se$. The average crystallite sizes of the samples were calculated using the Debye−Scherrer formula and were found to be 34, 25, 17, 8 and 12 nm for 4H, 8H, 12H, 16H, and 20H samples, respectively. Moreover, the crystallinity index of as-prepared materials was improved by increasing the reaction time.

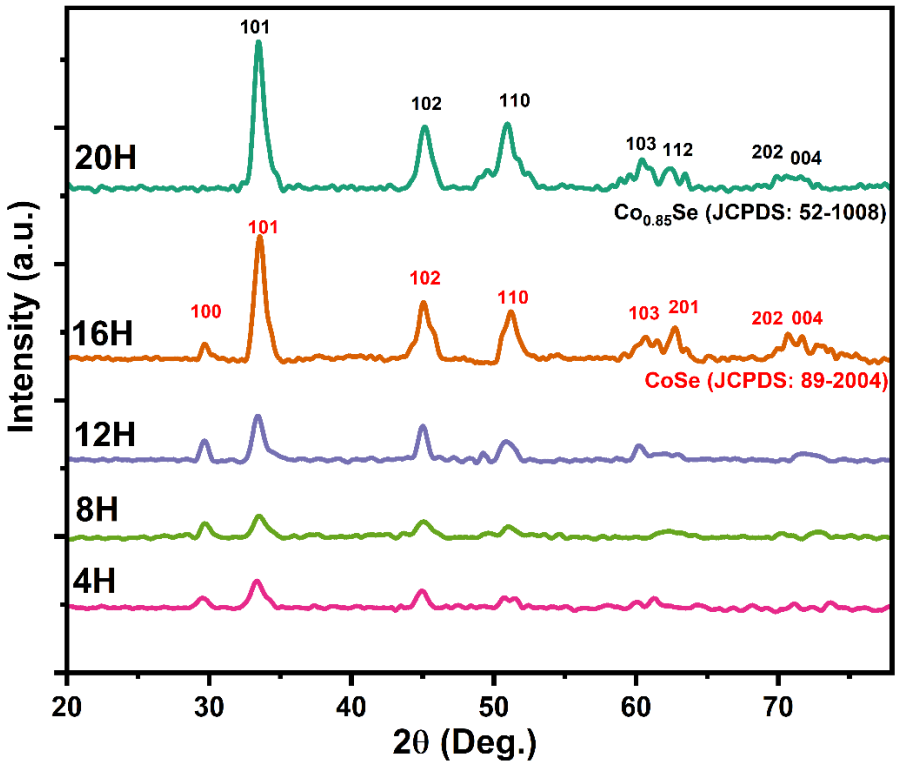

Figure 1: p-XRD patterns of 4H, 8H, 12H, 16H and 20H

The morphology of as-prepared materials was analysed by scanning electron microscopy (SEM). As the catalytic reactions takes place on the surface so morphologies of as-synthesized materials are very important. CoSe nanoparticles exhibit dendrimeric structure and these dendrimers are expected to facilitate transportation of electron which will promote OER The

SEM micrographs of best performing catalyst, 16H, show the dendrimeric structure of 20-30 nanometer diameter, as shown in Figure 2 (a-c). In addition, open channel cavities of several nanometer size can also be seen which are vital to enhance the mass diffusion process for efficient kinetics. In case of 20H, fusion of dendrimeric structures into larger particles with a diameter of 150-200 nm were observed, which reduce the active surface area of the catalyst (Figure S2 (d-f)). Aggregated micron-level sheet like structures can be seen in the images of sample 12H (Figure S2 (a-c)). The elemental contents of 16H were determined by energy dispersive X-ray (EDX) spectrometer, the atomic ratios of Co/Se were highly close to 1:1, which further validates the stoichiometric formation of CoSe. While in case of 20H, the contents of cobalt were significantly lower than the selenide (atomic ratio of Co/Se was 0.82:1) which indicates the presence of Co vacancies in 20H, as observed in its p-XRD pattern. This ratio is very close to empirical formula of $Co_{0.85}Se$ which further confirm its formation. The EDX elemental mapping of 16H shows the homogeneous distributation of both Co and Se throughout the matrix, as shown in Figure 2 .

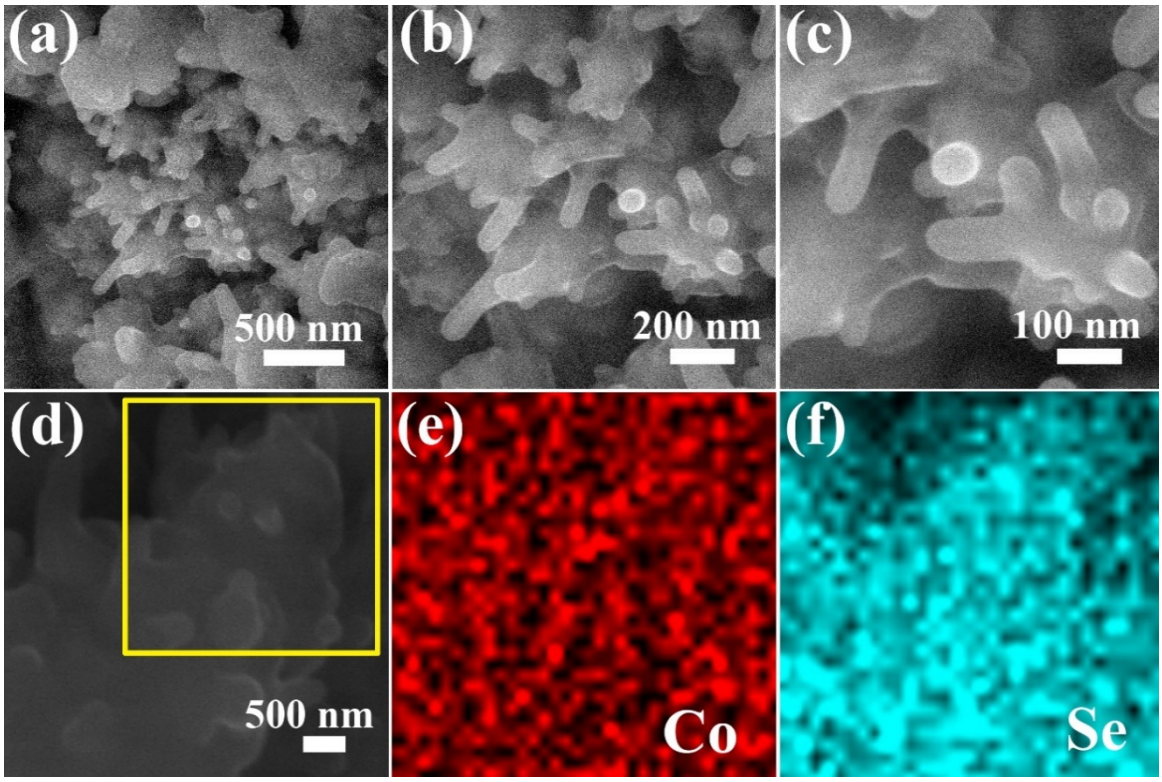

Figure 2 : (a)-(c) SEM images of dendrimer-like 16H; (d)-(f) Elemental mappings

Electrochemical performance of as-prepared materials for OER was evaluated in a three-electrode system, using standard calomel electrode and Pt as reference and counter electrode, respectively, with prepared materials coated on FTO as working electrodes. The LSV was performed for different catalysts in 1M KOH solution at a scan rate of 5 mV $s^{-1,}$ and the corresponding recorded curves are shown in Figure 3(a). To obtain the 10 $mAcm^{-2}$ electron density, the required overpotentials for 4H, 8H,12H, 16H and 20H were 360 mV, 290 mV, 280 mV, 250 mV, and 290 mV, respectively. All the prepared catalysts were found active for OER, and the LSV for 16H sample initiated OER at remarkably low overpotential and reaching very high current densities (570 $mAcm^{-2}$) for oxygen evolution reaction under a small potential window. This high catalytic activity of 16H sample is due to its high crystallinity, porosity and

dendrimeric morphology compared to other prepared materials, as evident by p-XRD patterns and SEM micrographs. The samples with other preparation times (4H and 8H) showed the least peak electron densities and the highest overpotentials due to their more amorphous nature and compact sheet-like morphologies. CoSe synthesized at 12 h time interval (that is 12H) and the sample prepared in 20 h time interval (that is 20H) showed almost similar results for the water oxidation reaction. The lower catalytic activity of 20H as compared to 16H sample is due to its phase change and aggolomerated morphology despite having better crystallinity than the 16H.

The kinetics of catalyst was examined by Tafel plots, which shows the effect of overpotential or potential on constant current density. Tafel plots of all prepared CoSe samples were investigated in the linear regions and fitted into the Tafel equation ($\eta = b\log J + a$) where b is Tafel slope. The resulting Tafel slopes for all prepared samples are shown in Figure 3(b). The Tafel slope of 16H sample is 56 mV dec^{-1}, smaller than all other prepared samples and benchmark RuO_2, implying an enhanced OER kinetics and improved bubble-releasing ability. These results suggest that high crystallinity, porous structure, dendrimeric morphology, and the hexagonal CoSe phase improved the mass transfer and boosted the electron transfer process in water oxidation. These features make 16H a suitable candidate in practical applications with more rapid OER rate. Linear sweep voltammograms were obtained at different scan rates of 5, 10, 25, 50, 75, 90 and 100 mVs^{-1} for 16H sample to investigate the scan rate effect on the current density and overpotential, as shown in Figure S3. The current density increased by increasing the scan rate, demonstrating rapid kinetics on the active electrode materials and low transport resistance between analyte and electrolyte for OER.

Electrochemical impedance spectroscopy (EIS) was conducted to understand better the kinetics of the OER process on prepared electrocatalysts. EIS was performed under a constant potential

of 0.5V and in the presence of 1.0 M KOH as an electrolyte. For each electrocatalytic experiment, a fresh electrolyte was used to minimize the differences in solution resistance. Figures 3(c, d) show the respective Nyquist EIS plots and the bar graph for the charge transfer resistances of all prepared electrocatalytic materials. A equivalent circuit was designed to fit the EIS data, as shown in the inset of Figure 3(c). The designed circuit comprised of three resistors R1, R2 and R3 and two other elements Yo5,a5 and Yo7, a7, from this circuit R_s and R_{ct} could be calculated. Solution resistance, R_s, is the resistance of the electrolyte, and R_{ct} is the charge transfer resistance which is the interfacial resistance between the electrocatalyst and the electrolyte [50]. As R_{ct} controls interfacial charge transfer kinetics which relates with the OER on the surface of catalyst. So, smaller value of R_{ct} leads to efficient OER reaction. EIS plot and bar graph of different prepared materials show that the 16H represents the lowest charge transfer resistance of just 0.218 Ω whereas the 4H showed highest charge transfer resistance of 5.07 Ω. The smallest charge transfer resistance for 16H among all other prepared materials suggests rapid kinetics and better catalytic activity. This difference in charge transfer resistances of as-synthesized materials shows that crystallinity, porosity and morphology play important roles in developing efficient electrocatalysts for water oxidation.

Electrochemically active surface area (ECSA) of all prepared materials was calculated using CV scans in the non-Faradic potential region at varied scanning rates (10 mV s^{-1}, 20 mV s^{-1}, 30 mV s^{-1}, 40 mV s^{-1}, 50 mV s^{-1}). A linear plot of scan rate versus capacitive current was derived from recorded CV data, and ther slope of this curve gave a quantitative value of double-layer capacitance (CdI). For these materials current linearly depends on the scan rate, which relates with capacittaive charging behaviour. The corresponding non-Faradic CV scans and linear plots for determination of CdI are shown in Figure S4. The magnitude of double-

layer capacitance is a measure of the ECSA. Abundant surface-active sites were found in 12H, 16H and 20H. The measured CdI values are 26.1, 20.4 and 17.5 mF cm^{-2} for 12H, 16H and 20H, respectively. From these values of CdI, ECSA were estimated and are shown in the form of bar graph in the Figure 3(e). The highest ECSA was observed for 16H followed by the 12H and then for 20H. This trend indicates that materials' phase, crystallinity, morphology and porosity are critical in bringing accessible reaction sites for water oxidation. The sample 20H is highly crystalline and porous, however, it has fewer active sites than 16H and 12H due to different CoSe phases and fusion of dendrimeric architectures. The results of ECSA suggests that 16H sample had more exposed Co sites, leading to formation of more Co active species as compared to other samples. Amorphous nature and micron-level sheet like structures leads to lowest ECSA for 4H followed by 8H. The ECSA results are in good agreement with other characterizations and electrochemical evaluations.

Besides fast kinetics and higher catalytic activities, stability of electrocatalyst is another essential criterion for commercial application. Chronopotentiometry of 16H sample was performed under constant current densities of 20 mA cm^{-2} and 50 $mAcm^{-2}$ for over 24 hours. A rich, continuous stream of oxygen bubbles were seen coming out of electrode surface during the chronopotentiometric tests. The material 16H showed sustain potential values for OER throughout the experiment, indicating its excellent stability under harsh oxidative conditions, as shown in Figure 3(f). The percentage retention of electrocatalyst was above 95 percent, and negligible increase in the overpotential was observed. A slight increase in voltage was observed in both potentiometric experiments that could be a result of small removal of electrocatalyst from the surface of electrode and decrease in contact between catalyst and

electrolyte due to continuous generation of oxygen gas. On the other hand, RuO_2 exhibit poor stability with continuous attenuation of current density and chronoamperometric response of RuO_2 was only 75 percent, as compared to initial current density under alkaline conditions. These results predicted that dendrimeric cobalt selenide is outstanding catalyst for OER.

After the stability test, LSV of 16H was again conducted and compared with the LSV curve of fresh 16H. Negligible changes in the current density and overpotential were observed in both LSV curves, as shown in the Figure S5. EIS of fresh 16H and after chronopotentiometric stability test was also conducted. As shown in the Figure S6 and S7, a small increase in resistance of 16H was observed after 24 hours stability test. These slight changes in current density and resistance of 16H after stability experiment could be due to poisoning of very few active sites under highly oxidative conditions. In addition, powder XRD was also performed before and after stability experiment and the resultant XRD patterns are shown in Figure S8. These patterns indicate that 16H ultimately retained its structure and the crystalline changes were imperceptible, further confirming its excellent stability.

The performance of reported cobalt selenides has been illustrated in table S1 which shows that present work exhibits best results. The excellent catalytic activity of as-synthesized catalyst could be attributed to following factor: (i) dendrimeric structure which facilitated electron transport (ii) increased Co active sites

Possible mechanism of OER in alkaline conditions has been described below [53]:-

$$Co(II) + 3OH^- \leftrightarrow Co(III)OOH + H_2O + e^- \quad (1)$$

$$Co(III)OOH + OH^- \leftrightarrow Co(IV)O(OH)_2 + e^- \quad (2)$$

$$Co(IV)O(OH)_2 + 2OH^- \leftrightarrow Co(IV)OO_2 + 2H_2O + 2e^- \quad (3)$$

272 $$Co(IV)OO_2 + OH^- \rightarrow Co(III)OOH + O_2 + e^- \quad (4)$$

273 Summary OER: $4OH^- \rightarrow O_2 + 2H_2O + 4e^-$

274 First three steps are reversible and explains entire OER process while fourth step is irreversible
275 and fast. Co^{+2} firstly oxidized on the surface of electrode and forms CoOOH/CoSe, then it is
276 oxidized to $CoOO_2$/CoSe, followed by its electrochemical oxidation and formation of O_2 and
277 CoOOH. Moreover, dendrimeric structure of CoSe provides larger surfacea area and more
278 active sites and enhance interfacial charge transfer which promotes OER reaction rate. Higher
279 surface area also increase interface contact between electrolyte and electrode.

280

281

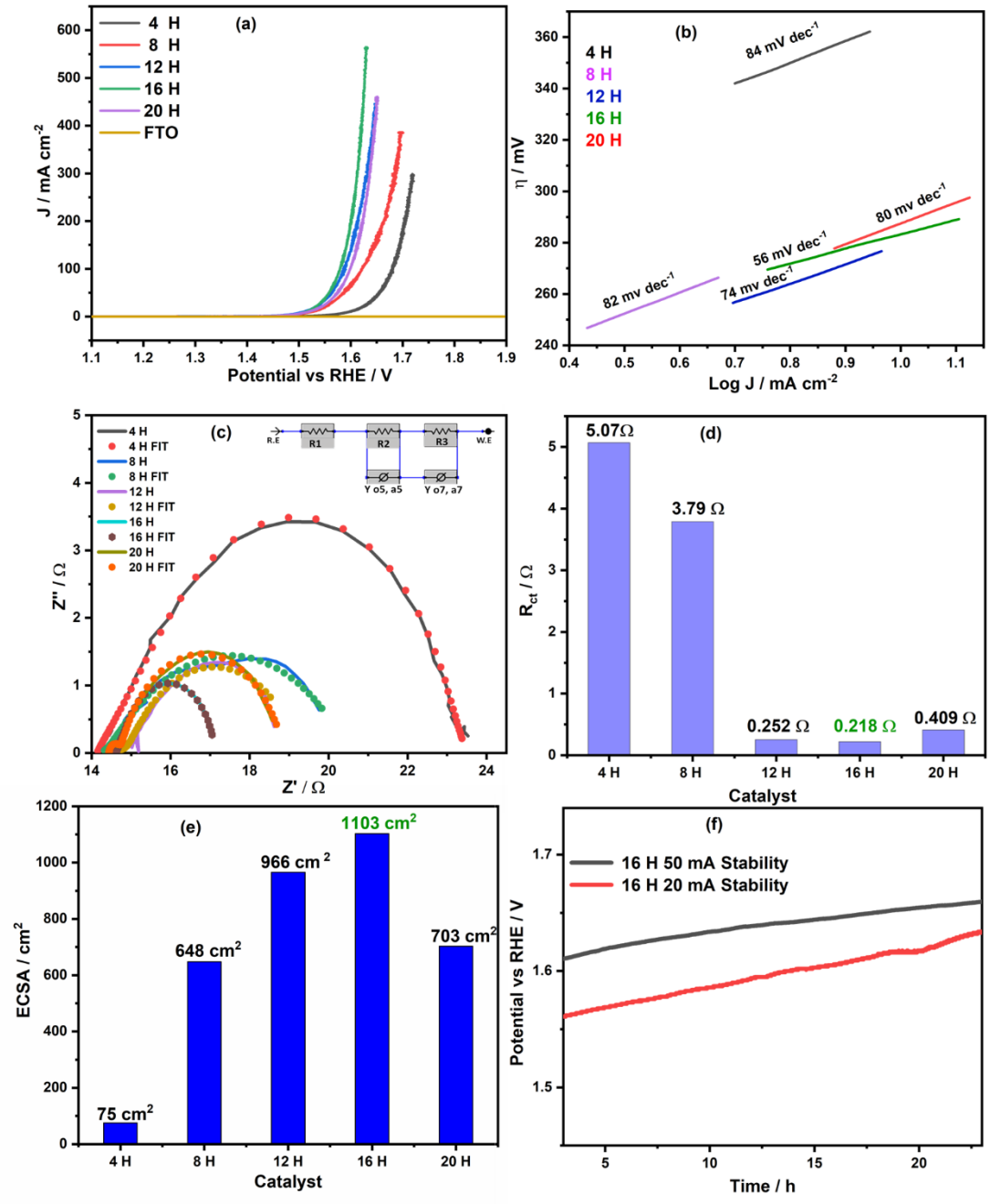

Figure 3 : Electrochemical studies of 4H, 8H, 12H, 16H and 20H (a) Linear sweep voltammograms (b) Tafel plots in the linear regions (c) Nyquist EIS plots (d) charge transfer resistances (e) Electrochemically active surface areas (f) chronopotentiometric tests under constant current densities of 20 mA cm^{-2} and 50 $mAcm^{-2}$ for over 24 hours

5. Conclusions

In summary, we have synthesized dendrimeric nanoparticles of cobalt selenide at different temperatures via hydrothermal method. It was observed that CoSe synthesized at 16H exhibits excellent electrochemical activity with remarkably low overpotential (250 mV at 10 mA cm^{-2}) and very high current density (570 mA cm^{-2}) in a small potential window. The Tafel slope of 16H sample was 56 mV dec^{-1} which indicates the faster kinetics at the catalyst surfaces. Moreover, it also showed excellent stability in harsh oxidative condition in a 24-hour long stability test under alkaline conditions. Benefiting from higher stability, large electrochemically active surface area, low overpotential and faster rate of electron transformation, cobalt selenide electrocatalyst performance exceeds from commercial electrocatalysts. To the best of our knowledge, the activity of as-synthesized catalyst is superior as compared to noble metal catalysts. The remarkable OER efficiency is attributed to crystallinity, porosity, morphology and nature of CoSe phase. It is important to note that crystalline and porous hexagonal CoSe is not only economical but also very stable electrocatalyst and this work paves pathways for preparation of selenide based, efficient OER catalyst by introducing different transition metals in it.

Credit authorship contribution statement

Muhammad Bilal: Experimental, Data curation, Writing original draft, Rashid: Data curation, Validation, Amna Altaf: Data curation, Write up, Nadeem Baig: Data curation, Ghayoor Abbas Chotana: Data curation, Raja Shahid Ashraf: Data curation, Shahid Rasool: Co-supervision, Editing, Ayman Nafadi: Data curation; Manzar Sohail: Supervision, Conceptulization Writing rereview & editing.

Declaration of competing interest

The authors declare that they have no known competing financial interests or personal relationships that could have appeared to influence the work reported in this paper.

Acknowledgements

This work was supported by the Higher Edication Commission, Pakistan (grant No. LCF 07).

Appendix A. Supplementary data Supplementary data to this article can be found online at …….

References

1. Koper, M. T. M., A basic solution. *Nature Chemistry* **2013,** *5* (4), 255-256.

2. Cobo, S.; Heidkamp, J.; Jacques, P.-A.; Fize, J.; Fourmond, V.; Guetaz, L.; Jousselme, B.; Ivanova, V.; Dau, H.; Palacin, S.; Fontecave, M.; Artero, V., A Janus cobalt-based catalytic material for electro-splitting of water. *Nature Materials* **2012,** *11* (9), 802-807.

3. Wang, J.; Zhang, Z.; Song, H.; Zhang, B.; Liu, J.; Shai, X.; Miao, L., Water Dissociation Kinetic-Oriented Design of Nickel Sulfides via Tailored Dual Sites for Efficient Alkaline Hydrogen Evolution. *Advanced Functional Materials* **2021,** *31* (9), 2008578.

4. Hong, W. T.; Risch, M.; Stoerzinger, K. A.; Grimaud, A.; Suntivich, J.; Shao-Horn, Y., Toward the rational design of non-precious transition metal oxides for oxygen electrocatalysis. *Energy & Environmental Science* **2015,** *8* (5), 1404-1427.

5. Lyu, F.; Bai, Y.; Li, Z.; Xu, W.; Wang, Q.; Mao, J.; Wang, L.; Zhang, X.; Yin, Y., Self-Templated Fabrication of CoO–MoO2 Nanocages for Enhanced Oxygen Evolution. *Advanced Functional Materials* **2017,** *27* (34), 1702324.

6. Kanan Matthew, W.; Nocera Daniel, G., In Situ Formation of an Oxygen-Evolving Catalyst in Neutral Water Containing Phosphate and Co2+. *Science* **2008,** *321* (5892), 1072-1075.

7. Tripkovic, V.; Hansen, H. A.; Vegge, T., From 3D to 2D Co and Ni Oxyhydroxide Catalysts: Elucidation of the Active Site and Influence of Doping on the Oxygen Evolution Activity. *ACS Catalysis* **2017,** *7* (12), 8558-8571.

8. Ramakrishnan, S.; Balamurugan, J.; Vinothkannan, M.; Kim, A. R.; Sengodan, S.; Yoo, D. J., Nitrogen-doped graphene encapsulated FeCoMoS nanoparticles as advanced trifunctional catalyst for water splitting devices and zinc–air batteries. *Applied Catalysis B: Environmental* **2020,** *279*, 119381.

9. Hou, Y.; Lohe, M. R.; Zhang, J.; Liu, S.; Zhuang, X.; Feng, X. J. E.; Science, E., Vertically oriented cobalt selenide/NiFe layered-double-hydroxide nanosheets supported on exfoliated graphene foil: an efficient 3D electrode for overall water splitting. **2016,** *9* (2), 478-483.

10. Petrykin, V.; Macounova, K.; Shlyakhtin, O. A.; Krtil, P., Tailoring the Selectivity for Electrocatalytic Oxygen Evolution on Ruthenium Oxides by Zinc Substitution. *Angewandte Chemie International Edition* **2010,** *49* (28), 4813-4815.

11. Lee, Y.; Suntivich, J.; May, K. J.; Perry, E. E.; Shao-Horn, Y., Synthesis and Activities of Rutile IrO2 and RuO2 Nanoparticles for Oxygen Evolution in Acid and Alkaline Solutions. *The Journal of Physical Chemistry Letters* **2012,** *3* (3), 399-404.

12. Kötz, R.; Neff, H.; Stucki, S., Anodic Iridium Oxide Films: XPS-Studies of Oxidation State Changes and. *Journal of The Electrochemical Society* **1984,** *131* (1), 72-77.

13. Kötz, R.; Lewerenz, H.; Stucki, S. J. J. o. T. E. S., XPS Studies of Oxygen Evolution on Ru and RuO2 Anodes. **1983,** *130*, 825-829.

14. Yan, Y.; Xia, B. Y.; Zhao, B.; Wang, X., A review on noble-metal-free bifunctional heterogeneous catalysts for overall electrochemical water splitting. *Journal of Materials Chemistry A* **2016,** *4* (45), 17587-17603.

15. Li, Y.-X.; Han, Y.-C.; Wang, C.-C. J. C. E. J., Fabrication strategies and Cr (VI) elimination activities of the MOF-derivatives and their composites. **2021,** *405*, 126648.

16. Plevová, M.; Hnát, J.; Bouzek, K., Electrocatalysts for the oxygen evolution reaction in alkaline and neutral media. A comparative review. *Journal of Power Sources* **2021,** *507*, 230072.

17. Lyu, F.; Wang, Q.; Choi, S. M.; Yin, Y., Noble-Metal-Free Electrocatalysts for Oxygen Evolution. *Small* **2019,** *15* (1), 1804201.

18. Zhao, C.-X.; Liu, J.-N.; Wang, J.; Ren, D.; Li, B.-Q.; Zhang, Q., Recent advances of noble-metal-free bifunctional oxygen reduction and evolution electrocatalysts. *Chemical Society Reviews* **2021,** *50* (13), 7745-7778.

19. Lv, L.; Gan, Y.; Wan, H.; Li, Z.; Wang, C.; Wang, H., Electronic coupling regulation in yolk-shell nanostructured nickel-cobalt diselenides with octahedral coordination for boosted oxygen evolution reaction. *International Journal of Hydrogen Energy* **2021,** *46* (56), 28387-28396.

20. Sobhani, A.; Salavati-Niasari, M. J. J. o. M. L., Cobalt selenide nanostructures: Hydrothermal synthesis, considering the magnetic property and effect of the different synthesis conditions. **2016,** *219*, 1089-1094.

21. Zhu, G.; Xie, X.; Li, X.; Liu, Y.; Shen, X.; Xu, K.; Chen, S., Nanocomposites Based on CoSe2-Decorated FeSe2 Nanoparticles Supported on Reduced Graphene Oxide as High-Performance Electrocatalysts toward Oxygen Evolution Reaction. *ACS Applied Materials & Interfaces* **2018,** *10* (22), 19258-19270.

22. Zare, A.; Bayat, A.; Saievar-Iranizad, E.; Naffakh-Moosavy, H., One step preparation of Fe doped CoSe2 supported on nickel foam by facile electrodeposition method as a highly efficient oxygen evolution reaction electrocatalyst. *Journal of Electroanalytical Chemistry* **2020,** *878*, 114595.

23. Wang, S.; He, P.; Jia, L.; He, M.; Zhang, T.; Dong, F.; Liu, M.; Liu, H.; Zhang, Y.; Li, C.; Gao, J.; Bian, L., Nanocoral-like composite of nickel selenide nanoparticles anchored on two-dimensional multi-layered graphitic carbon nitride: A highly efficient electrocatalyst for oxygen evolution reaction. *Applied Catalysis B: Environmental* **2019,** *243*, 463-469.

24. Zhang, J.-Y.; Yan, Y.; Mei, B.; Qi, R.; He, T.; Wang, Z.; Fang, W.; Zaman, S.; Su, Y.; Ding, S.; Xia, B. Y., Local spin-state tuning of cobalt–iron selenide nanoframes for the boosted oxygen evolution. *Energy & Environmental Science* **2021,** *14* (1), 365-373.

25. Poorahong, S.; Harding, D. J.; Keawmorakot, S.; Siaj, M., Free standing bimetallic nickel cobalt selenide nanosheets as three-dimensional electrocatalyst for water splitting. *Journal of Electroanalytical Chemistry* **2021,** *897*, 115568.

26. Masud, J.; Swesi, A. T.; Liyanage, W. P. R.; Nath, M., Cobalt Selenide Nanostructures: An Efficient Bifunctional Catalyst with High Current Density at Low Coverage. *ACS Applied Materials & Interfaces* **2016,** *8* (27), 17292-17302.

27. Ren, H.; Yu, L.; Yang, L.; Huang, Z.-H.; Kang, F.; Lv, R., Efficient electrocatalytic overall water splitting and structural evolution of cobalt iron selenide by one-step electrodeposition. *Journal of Energy Chemistry* **2021,** *60*, 194-201.

28. Ao, K.; Dong, J.; Fan, C.; Wang, D.; Cai, Y.; Li, D.; Huang, F.; Wei, Q., Formation of Yolk–Shelled Nickel–Cobalt Selenide Dodecahedral Nanocages from Metal–Organic Frameworks for Efficient Hydrogen and Oxygen Evolution. *ACS Sustainable Chemistry & Engineering* **2018,** *6* (8), 10952-10959.

29. Masud, J.; Liyanage, W. P. R.; Cao, X.; Saxena, A.; Nath, M., Copper Selenides as High-Efficiency Electrocatalysts for Oxygen Evolution Reaction. *ACS Applied Energy Materials* **2018,** *1* (8), 4075-4083.

30. Zheng, X.; Zhang, J.; Wang, J.; Zhang, Z.; Hu, W.; Han, Y., Facile synthesis of nickel cobalt selenide hollow nanospheres as efficient bifunctional electrocatalyst for rechargeable Zn-air battery. *Science China Materials* **2020,** *63* (3), 347-355.

31. Xia, L.; Song, H.; Li, X.; Zhang, X.; Gao, B.; Zheng, Y.; Huo, K.; Chu, P. K., Hierarchical 0D−2D Co/Mo Selenides as Superior Bifunctional Electrocatalysts for Overall Water Splitting. **2020,** *8* (382).

32. Chae, S.-H.; Muthurasu, A.; Kim, T.; Kim, J. S.; Khil, M.-S.; Lee, M.; Kim, H.; Lee, J. Y.; Kim, H. Y., Templated fabrication of perfectly aligned metal-organic framework-supported iron-doped copper-

cobalt selenide nanostructure on hollow carbon nanofibers for an efficient trifunctional electrode material. *Applied Catalysis B: Environmental* **2021,** *293*, 120209.

33. Dai, J.; Zhao, D.; Sun, W.; Zhu, X.; Ma, L.-J.; Wu, Z.; Yang, C.; Cui, Z.; Li, L.; Chen, S., Cu(II) Ions Induced Structural Transformation of Cobalt Selenides for Remarkable Enhancement in Oxygen/Hydrogen Electrocatalysis. *ACS Catalysis* **2019,** *9* (12), 10761-10772.

34. Zeng, C.; Dai, L.; Jin, Y.; Liu, J.; Zhang, Q.; Wang, H., Design strategies toward transition metal selenide-based catalysts for electrochemical water splitting. *Sustainable Energy & Fuels* **2021,** *5* (5), 1347-1365.

35. Cao, X.; Johnson, E.; Nath, M., Expanding Multinary Selenide Based High-Efficiency Oxygen Evolution Electrocatalysts through Combinatorial Electrodeposition: Case Study with Fe–Cu–Co Selenides. *ACS Sustainable Chemistry & Engineering* **2019,** *7* (10), 9588-9600.

36. Anantharaj, S.; Ede, S. R.; Sakthikumar, K.; Karthick, K.; Mishra, S.; Kundu, S., Recent Trends and Perspectives in Electrochemical Water Splitting with an Emphasis on Sulfide, Selenide, and Phosphide Catalysts of Fe, Co, and Ni: A Review. *ACS Catalysis* **2016,** *6* (12), 8069-8097.

37. Zhang, J.-Y.; Lv, L.; Tian, Y.; Li, Z.; Ao, X.; Lan, Y.; Jiang, J.; Wang, C., Rational Design of Cobalt–Iron Selenides for Highly Efficient Electrochemical Water Oxidation. *ACS Applied Materials & Interfaces* **2017,** *9* (39), 33833-33840.

38. Zhang, C.; Xin, B.; Duan, S.; Jiang, A.; Zhang, B.; Li, Z.; Hao, J. J. C. A. A. J., Controllable 1D and 2D cobalt oxide and cobalt selenide nanostructures as highly efficient electrocatalysts for the oxygen evolution reaction. **2018,** *13* (18), 2700-2707.

39. Liu, X.; Liu, Y.; Fan, L.-Z., MOF-derived CoSe2 microspheres with hollow interiors as high-performance electrocatalysts for the enhanced oxygen evolution reaction. *Journal of Materials Chemistry A* **2017,** *5* (29), 15310-15314.

426 40. Feng, Z.; Gao, B.; Wang, L.; Zhang, H.; Lu, P.; Xing, P., Nanoporous Cobalt-Selenide as High-
427 Performance Bifunctional Electrocatalyst towards Oxygen Evolution and Hydrazine Oxidation. *Journal of*
428 *The Electrochemical Society* **2020,** *167* (13), 134501.
429 41. Kwak, I. H.; Im, H. S.; Jang, D. M.; Kim, Y. W.; Park, K.; Lim, Y. R.; Cha, E. H.; Park, J., CoSe2 and
430 NiSe2 Nanocrystals as Superior Bifunctional Catalysts for Electrochemical and Photoelectrochemical
431 Water Splitting. *ACS Applied Materials & Interfaces* **2016,** *8* (8), 5327-5334.
432 42. Liu, Y.; Cheng, H.; Lyu, M.; Fan, S.; Liu, Q.; Zhang, W.; Zhi, Y.; Wang, C.; Xiao, C.; Wei, S.; Ye, B.;
433 Xie, Y., Low Overpotential in Vacancy-Rich Ultrathin CoSe2 Nanosheets for Water Oxidation. *Journal of*
434 *the American Chemical Society* **2014,** *136* (44), 15670-15675.
435 43. Ghosh, S.; Tudu, G.; Mondal, A.; Ganguli, S.; Inta, H. R.; Mahalingam, V., Inception of Co3O4 as
436 Microstructural Support to Promote Alkaline Oxygen Evolution Reaction for Co0.85Se/Co9Se8 Network.
437 *Inorganic Chemistry* **2020,** *59* (23), 17326-17339.
438 44. Zhao, Y.; Jin, B.; Zheng, Y.; Jin, H.; Jiao, Y.; Qiao, S. Z. J. A. E. M., Charge state manipulation of
439 cobalt selenide catalyst for overall seawater electrolysis. **2018,** *8* (29), 1801926.
440 45. Li, W.; Gao, X.; Xiong, D.; Wei, F.; Song, W.-G.; Xu, J.; Liu, L., Hydrothermal Synthesis of
441 Monolithic Co3Se4 Nanowire Electrodes for Oxygen Evolution and Overall Water Splitting with High
442 Efficiency and Extraordinary Catalytic Stability. *Advanced Energy Materials* **2017,** *7* (17), 1602579.
443 46. Ganguli, S.; Ghosh, S.; Tudu, G.; Koppisetti, H. V. S. R. M.; Mahalingam, V., Design Principle of
444 Monoclinic NiCo2Se4 and Co3Se4 Nanoparticles with Opposing Intrinsic and Geometric Electrocatalytic
445 Activity toward the OER. *Inorganic Chemistry* **2021,** *60* (13), 9542-9551.
446 47. Zhang, J.; Xu, Q.; Hu, Y.; Jiang, H.; Li, C., Selenium vacancy triggered atomic disordering of
447 Co0.85Se nanoparticles towards a highly-active electrocatalyst for water oxidation. *Chemical*
448 *Communications* **2020,** *56* (92), 14451-14454.

449 48. Zhong, Q.-S.; Xia, W.-Y.; Liu, B.-C.; Xu, C.-W.; Li, N., Co0.85Se on three-dimensional hierarchical
450 porous graphene-like carbon for highly effective oxygen evolution reaction. *International Journal of*
451 *Hydrogen Energy* **2019,** *44* (21), 10182-10189.
452 49. Liao, M.; Zeng, G.; Luo, T.; Jin, Z.; Wang, Y.; Kou, X.; Xiao, D., Three-dimensional coral-like cobalt
453 selenide as an advanced electrocatalyst for highly efficient oxygen evolution reaction. *Electrochimica*
454 *Acta* **2016,** *194*, 59-66.
455 50. Masud, J.; Swesi, A. T.; Liyanage, W. P.; Nath, M. J. A. a. m.; interfaces, Cobalt selenide
456 nanostructures: an efficient bifunctional catalyst with high current density at low coverage. **2016,** *8* (27),
457 17292-17302.
458 51. Panneerselvam, A.; Nguyen, C. Q.; Waters, J.; Malik, M. A.; O'Brien, P.; Raftery, J.; Helliwell, M. J.
459 D. T., Ligand influence on the formation of P/Se semiconductor materials from metal–organic
460 complexes. **2008,** (33), 4499-4506.
461 52. Holder, C. F.; Schaak, R. E. J. A. N., Tutorial on powder X-ray diffraction for characterizing
462 nanoscale materials. ACS Publications: 2019; Vol. 13, pp 7359-7365.
463 53. Liao, M.; Zeng, G.; Luo, T.; Jin, Z.; Wang, Y.; Kou, X.; Xiao, D. J. E. A., Three-dimensional coral-like
464 cobalt selenide as an advanced electrocatalyst for highly efficient oxygen evolution reaction. **2016,** *194*,
465 59-66.

466